Experimental

Chemicals

Chloroplatinic acid hexahydrate ($H_2PtCl_6 \cdot 6H_2O$), N-Methyl pyrrolidone (NMP), ethanol, methanol, perchloric acid, and sodium hydroxide (NaOH) were all purchased from Tianjin Fengchuan chemical reagent technology Ltd. Copper (II) chloride dihydrate ($CuCl_2 \cdot 2H_2O$) and carbon-supported Pt catalyst (Pt/C-JM, 20 wt.%) were obtained from Sinopharm Chemical Reagent Co Ltd. All reagents were analytical grade and used without further treatments. Deionized water was used for all experiments.

Synthesis of PtCu aerogel

In general, 70 μL $CuCl_2 \cdot 2H_2O$ (0.6 mol), 2 mL $H_2PtCl_6 \cdot 6H_2O$ (20 mmol), 10 mg NaOH, 5 mL NMP and 3mL deionized water were mixed and stirred at ambient temperature for 30 min. Then, the homogeneous solution was obtained and transferred to a 20 mL autoclave and heated at 180 °C for 8 h. After cooling to room temperature, the obtained PtCu aerogels were centrifuged and washed several times with deionized water and ethanol. The product was then dried in a vacuum oven at 70 °C for 8 h.

Characterization

The crystal structure and crystallinity of catalyst were performed on a PuXi XD3 diffractometer (Cu Kα, λ=0.15406 nm). The valence states and compositions were measured on a PHI-5000 X-ray photoelectron spectroscopy (XPS) using Al Kα radiation. A JEOL-2100F apparatus obtained transmission electron microscopy (TEM) and elemental mapping results at 200 kV. A high-resolution TEM (HRTEM) image was carried out on an FEI Tecnai G2F30 apparatus at 300 kV.

Electrochemical measurements

Electrochemical measurement was carried out by a three-electrode system. The graphite rod, Ag/AgCl (3 M), and glassy carbon (3.0 mm in diameter) were used as a counter electrode, reference electrode, and working electrode, respectively. 5 mg of catalyst was added into 1 mL of a mixture of ethanol, deionized water, and Nafion (5%) solution to form an ink (V_{Nafion}: V_{water}: $V_{ethanol}$ =30: 10: 1). Then 2 μL of the ink was smeared onto the working electrode.

Methanol oxidation reaction (MOR) measurement: Voltammetric measurements were performed on a CHI 760E electrochemical workstation with a three-electrode system. The glassy carbon, Ag/AgCl (3 M), and graphite rod were used as working electrode, reference electrode, and counter electrode, respectively. Before each experiment, the electrode potential was cycled from -0.2 V to 1.0 V vs. Ag/AgCl at a scan rate of 200 mV·s^{-1} until a stable voltammogram was obtained in N$_2$-saturated 0.5 M H$_2$SO$_4$ solution. The electrochemically active surface area (ECSA) of the catalyst was determined based on calculating the hydrogen under the potential desorption (Hupd) area of the CVs. The ECSA of the catalyst can be calculated by the following equation:

$$ECSA = \frac{Q}{C \times m}$$

where Q is the charge passed during the hydrogen adsorption/desorption from the electrode surface after the double layer correction, C (210 mC·cm^{-2}) is the charge needed to oxidize a monolayer of H$_2$ on the Pt catalyst, and m represents the amount of Pt on the electrode surface (mg), respectively. After potential cycling, CVs for the MOR were obtained from -0.2 V to 1.0 V at a scan rate of 100 mV·s^{-1}. The N$_2$-saturated 0.5 M H$_2$SO$_4$ and 1.0 M methanol solutions were used as the testing solution.

Chronoamperometry measurements were performed at a fixed potential for 4000 s in a solution containing 0.5 M H$_2$SO$_4$ + 1.0 M CH$_3$OH. For each catalyst, the current was normalized to the loading of noble metals (Pt) to obtain mass activity. All experiments were conducted at room temperature.

Oxygen reduction reaction (ORR) measurement: ORR measurements were performed on a CHI 760E electrochemical workstation with a three-electrode system. The glassy carbon, Ag/AgCl (3 M), and graphite rod were used as working electrode, reference electrode, and counter electrode, respectively. Before each experiment, the electrode potential was cycled from 0.9 V to -0.2 V vs. Ag/AgCl at a scan rate of 200 mV·s^{-1} until a stable voltammogram was obtained in N$_2$-saturated 0.1 M HClO$_4$ solution. The ORR performance was investigated by cyclic voltammetry (CV) in N$_2$-

saturated 0.1 M HClO$_4$ at a scan rate of 100 mV·s^{-1} at room temperature. Linear sweep voltammetry (LSV) was performed in the potential range from 0.9 to -0.2 V vs. Ag/AgCl at various rotation rates (400-2000 rpm) in 0.1 M HClO$_4$ under constant O$_2$ gas flow, with a total rate of 10 mV·s^{-1}. The potentials can be converted into reversible hydrogen electrode (RHE) according to the following equation:

$$E_{RHE} = E_{appl} + E_{Ag/AgCl} + 0.059 \text{ pH}$$

The corresponding Koutecky–Levich plots were analyzed at different potentials. The slopes of the linear fitting lines were used to calculate the number of transferred electrons (n) by the following Koutecky–Levich equation:

$$\frac{1}{j} = \frac{1}{j_k} + \frac{1}{j_d} = \frac{j}{j_k} + \frac{1}{B\varpi^{1/2}}$$

$$B = 0.62nFC_0D_0^{2/3}v^{-1/6}$$

where j is the measured current, j$_k$ is the kinetic current, j$_d$ is the diffusion-limiting current, w is the rotating speed, n is the number of transferred electrons, F is the Faraday constant (96485 C·mol^{-1}), C$_0$ is the oxygen solubility (1.2×10^{-3} mol·L^{-1}), D$_0$ is the oxygen diffusivity (1.93×10^{-5} cm^2·s^{-1}), and v is the kinetic viscosity of the electrolyte (0.01 cm^2·s^{-1}). The accelerated stability test (ADT) was carried out in 0.1 M HClO$_4$ from 0.9 V and -0.2 V at a scan rate of 200 mV·s^{-1} for 30000 cycles.

CO-stripping voltammograms were obtained by immersing the electrode in a CO-saturated 0.1 M HClO$_4$ solution under a CO blanket for 30 min at a scan rate of 50 mV·s^{-1}, running up from 0.9 to -0.2 V at 50 mV·s^{-1}. It can be used to calculate the electrochemically active surface area (ECSA) of the catalyst. For each catalyst, the current was normalized to the area amount of Pt to obtain specific activity, and all of the potentials recorded in this part are given with respect to a reversible hydrogen electrode (RHE) by related calculations. All experiments were conducted at room temperature.

The electron transfer number (n) and the peroxide yield (%H$_2$O$_2$) could be calculated as follows:

$$n = \frac{4I_D}{(I_D N + I_R/N)}$$

$$\%H_2O_2 = \frac{200I_R}{(I_RN + I_R)}$$

where I_D is the disk current, I_R is the ring current, and N = 0.4286 is the current collection efficiency of the Pt ring.

Computational details

All the calculations were performed by using Materials Studio (MS) based on plane-wave density functional theory (DFT). The exchange-correlation functional was described within the GGA parametrized by the Perdew-Burke-Ernzerhof [42]. The unit cell with a Γ-centered in the first Brillouin zone and uniform $3 \times 3 \times 1$ grid of kpoints sampling were used. Full geometry optimization was conducted by minimizing the kinetic energy cutoff of 500 eV without applying any symmetry. Additionally, the energy converges to 10^{-5} eV when the atom's position was relaxed. The charge density differences was investigated with the model of the considered the on the (111) surface of PtCu without nitrogen modification and PtCu with nitrogen modification, respectively, and the thickness at 3 layers bottom was fixed.
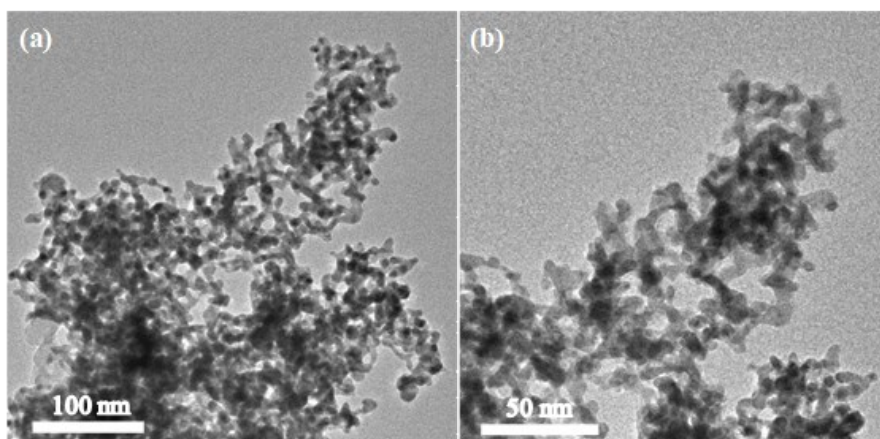
Fig. S1 (a, b) TEM images with different magnifications of PtCu.
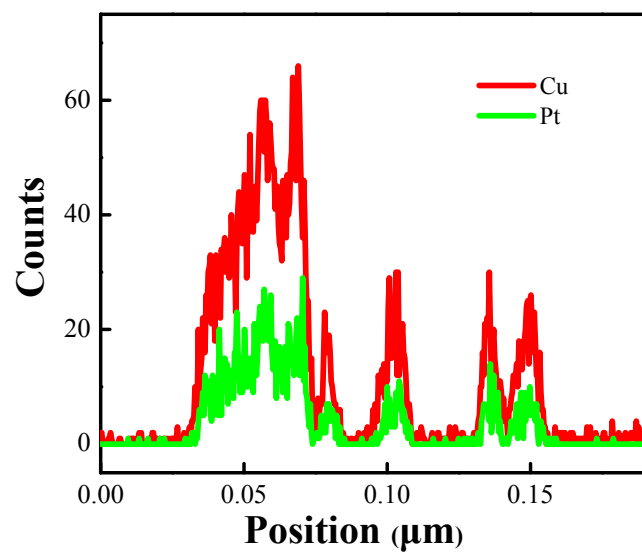
Fig. S2 The line scanning of PtCu.
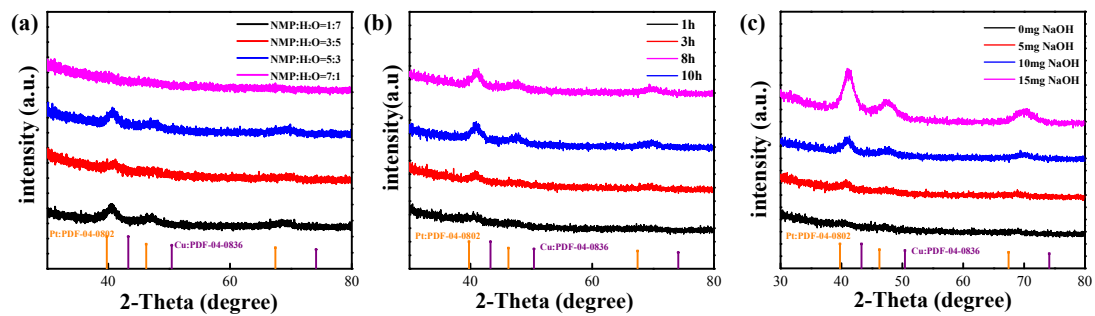
Fig. S3 XRD patterns of PtCu catalysts prepared with different synthesis conditions.
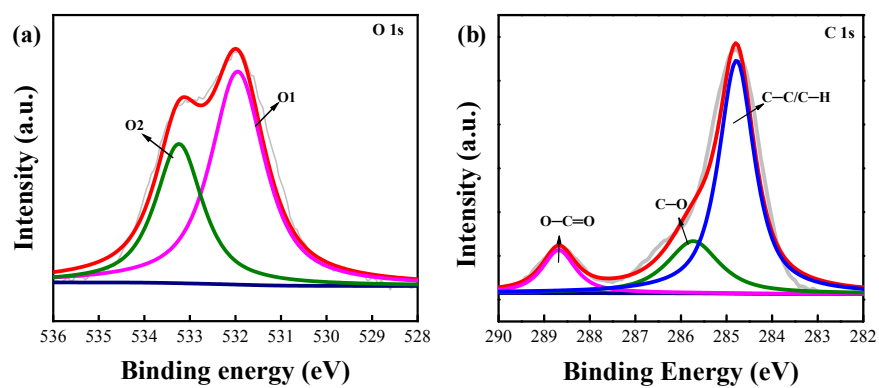
Fig. S4 XPS spectra of PtCu aerogels catalysts: (a) O 1s and (b) C 1s.
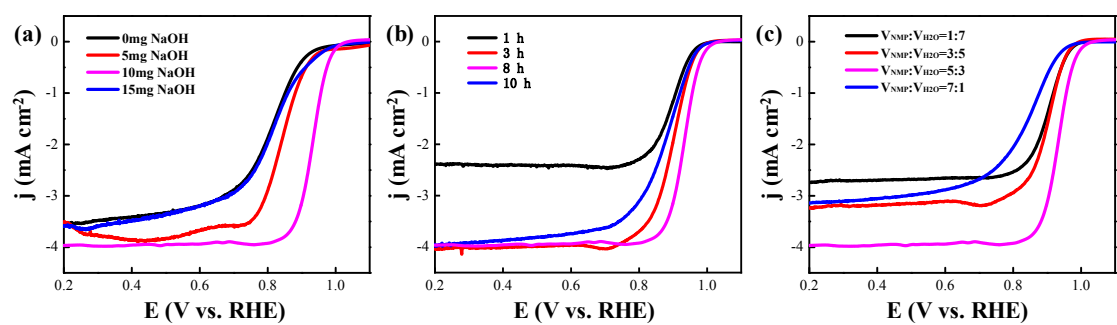
Fig. S5 Oxygen reduction polarization curves of PtCu catalysts prepared under different reaction conditions.
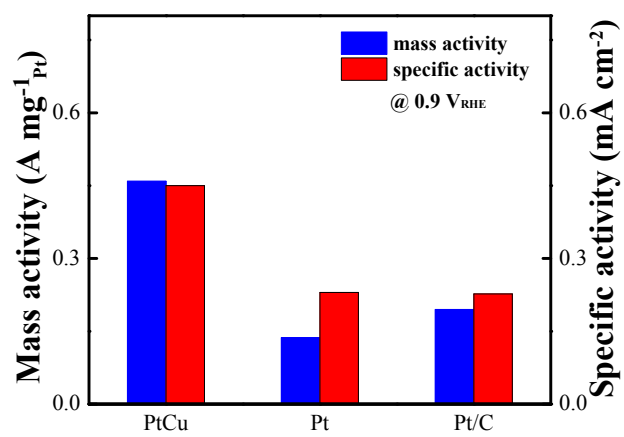
Fig. S6 Specific activity and mass activity of PtCu at 0.9 V$_{RHE}$.
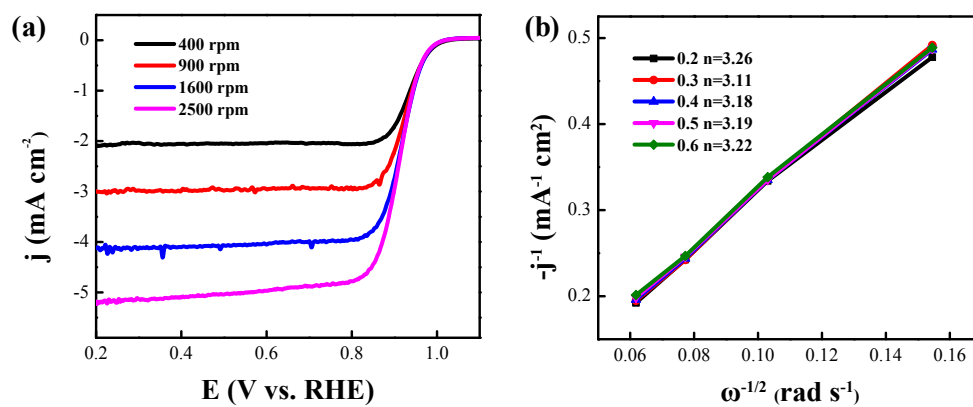
Fig. S7 ORR polarization of PtCu: (a) at different rotation rates, (b) the number of transferred electrons at different potentials.
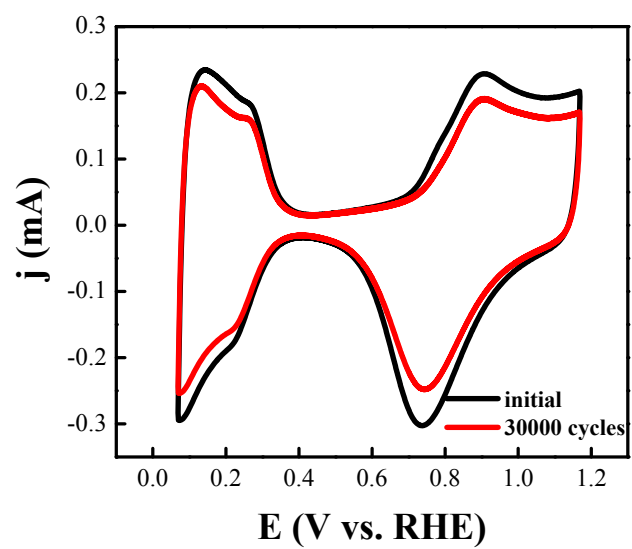
Fig. S8 CV of the PtCu before and after stability test for 30,000 cycles.
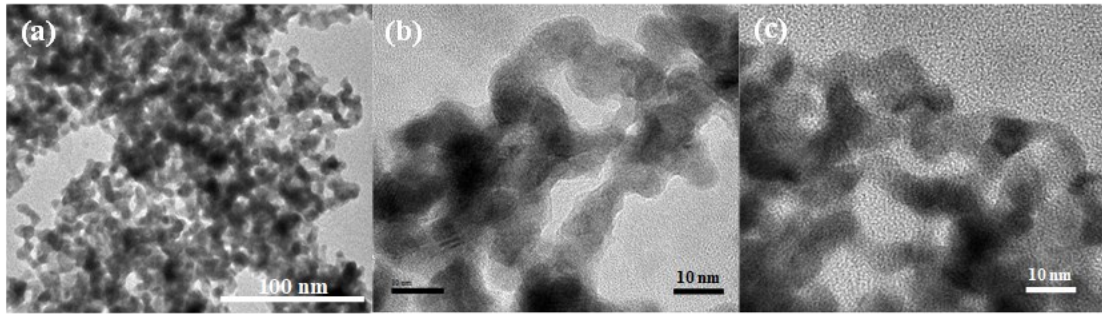
Fig. S9 TEM images of PtCu catalysts after stability test.
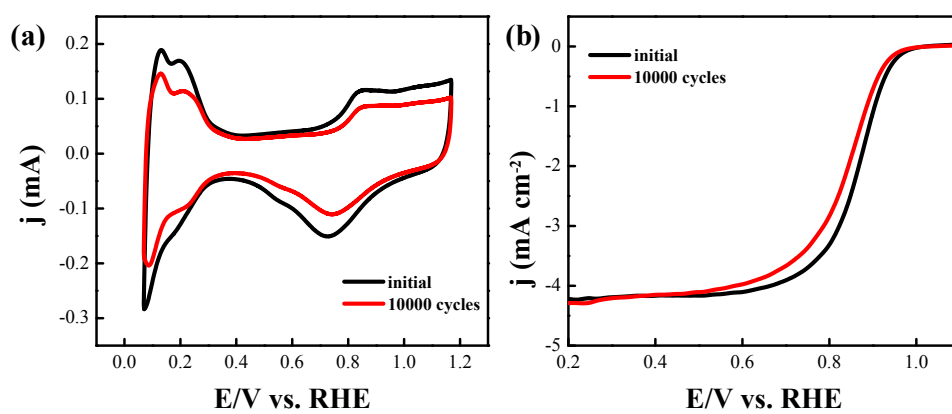
Fig. S10 CV and LSV of the commercial Pt/C before and after stability test for 10,000 cycles.
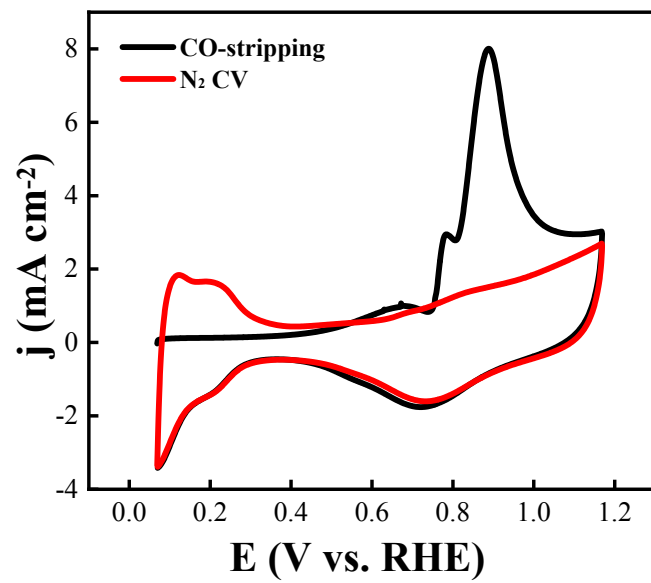
Fig. S11 CO-stripping test of the commercial Pt/C.
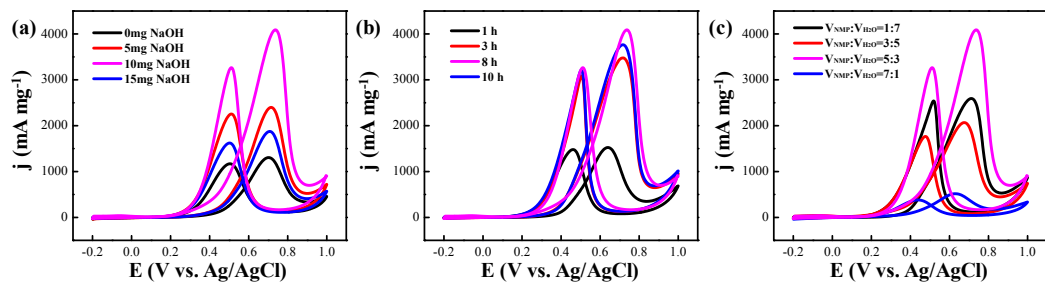
Fig. S12 MOR mass activity of PtCu catalysts prepared under different reaction conditions.
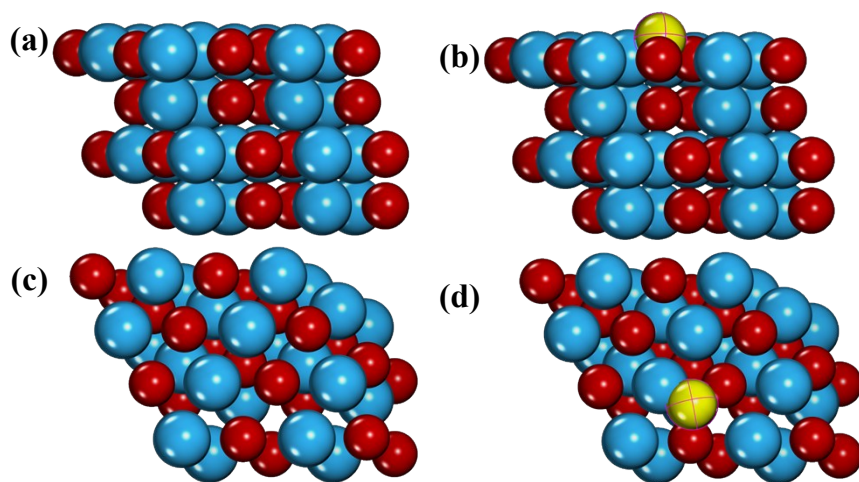
Fig. S13 Simulated diagram (a, c) PtCu without nitrogen modification and (b, d) PtCu with nitrogen modification (blue: Pt, red: Cu, yellow: N).

Table S1. The atomic percentage of different elements in various catalysts.

	Pt(at.%)	Cu(at.%)	N(at.%)	O(at.%)	C(at.%)
PtCu	4.54	3.21	2.04	20.2	70.01

Table S2. Summary of literature catalytic parameters of various Pt-based MOR catalyst.

Catalysts	Electrolyte	MA (A mg$_{Pt}^{-1}$)	SA (mA cm$_{Pt}^{-2}$)	Ref.
PtCu	0.5 M H$_2$SO$_4$ + 1.0 M CH$_3$OH	4.08	2.72	This work
Pt$_{17}$Pd$_{16}$Ru$_{22}$Te$_{45}$ NTs	0.5 M H$_2$SO$_4$ + 1.0 M CH$_3$OH	1.2615	2.96	1
PtPb(CNCs)	0.1 M HClO$_4$ + 0.5 M CH$_3$OH	0.97	2.09	2
Pt/TiN/CC	0.5 M H$_2$SO$_4$ + 1.0 M CH$_3$OH	1.670	1.63	3
PtRuCu/C	0.1 M HClO$_4$ + 1.0 M CH$_3$OH	1.35	5.22	4
Pt$_{69}$Ni$_{16}$Rh$_{15}$ NWs/C	0.1 M HClO$_4$ + 0.5 M CH$_3$OH	1.72	2.49	5
PtZn/MWNT-E	0.5 M H$_2$SO$_4$ + 1.0 M CH$_3$OH	0.59	1.02	6
PtNi CNCs	0.5 M H$_2$SO$_4$ + 0.5 M CH$_3$OH	0.696	1.37	7
Pt NP/LDG	1.0 M H$_2$SO$_4$ + 2.0 M CH$_3$OH	0.5962	--	8
Pt/H-TiO$_2$@NHPCN-800	0.5 M H$_2$SO$_4$ + 1.0 M CH$_3$OH	0.695	1.13	9
grapheme-MWCNTs/Pt	0.5 M H$_2$SO$_4$ + 1.0 M CH$_3$OH	0.16825	--	10
Ce-modified Pt NPs/C	0.5 M H$_2$SO$_4$ + 0.5 M CH$_3$OH	1.47	--	11
PtRu nanowires	0.1 M HClO$_4$ + 1.0 M CH$_3$OH	0.82	1.16	12
PtCo@NCs	0.1 M HClO$_4$ + 1.0 M CH$_3$OH	2.3	5.14	13
Pt$_3$CoRu/C@NC	0.1 M HClO$_4$ + 0.5 M CH$_3$OH	0.97	1.60	14
Au@CeO$_2$@Pt/	0.25 M H$_2$SO$_4$ + 1.0 M CH$_3$OH	1.36	1.72	15

C

Table S3. Summary of literature catalytic parameters of various Pt-based ORR catalysts.

Catalysts	$E_{1/2}$ V vs. RHE	MA @ 0.9V (A mg_{Pt}^{-1})	SA @0.9V (mA cm_{Pt}^{-2})	Ref.
PtCu	0.932	0.459	0.45	This work
Pt$_{1.1}$/BPdefect	<0.9	--	--	16
PtNi frame	--	0.24	0.44	17
Pt1@Pt/NBP	0.867	0.241	0.62	18
Pt$_1$-N/BP	0.76	--	--	19
PtCo/C-700	0.91	0.5	0.63	20
Pt@mPt CBNs	0.9	--	0.89	21
Pt$_{93}$Co/C	0.877	0.157	0.189	22
Pt/40Co-NC-900	0.92	<0.3	1.15	23
PtML/PdNS/ WNi/C	0.895	0.37	--	24
Pd-Pt nanoframes	--	0.40	0.75	25
PtNiCo@C-N NCs	0.84	--	--	26
HP-Ag/Pt	0.9	0.438	0.473	27

References

1 S. Y. Ma, H. H. Li, B. C. Hu, X. Cheng, Q. Q. Fu and S. H. Yu, J. Am. Chem. Soc., 2017, **139**, 5890-5895.

2 L. Huang, X. P. Zhang, Y. J. Hang, Q. Q. Wang, Y. X. Fang and S. J. Dong, Chem. Mat., 2017, **29**, 4557-4562.

3 J. Sun, X. Wang, Y. Song, Q. Wang, Y. Song, D. Yuan and L. Zhang, Chem. Commun., 2019, **55**, 13283-13286.

4 S. Xue, W. Deng, F. Yang, J. Yang, I. S. Amiinu, D. He, H. Tang and S. Mu, ACS Catal., 2018, **8**, 7578-7584.

5 W. Zhang, Y. Yang, B. Huang, F. Lv, K. Wang, N. Li, M. Luo, Y. Chao, Y. Li, Y. Sun, Z. Xu, Y. Qin, W. Yang, J. Zhou, Y. Du, D. Su and S. Guo, Adv. Mater., 2019, **31**, 1805833-1805842.

6 Z. Qi, C. Xiao, C. Liu, T. W. Goh, L. Zhou, R. Maligal-Ganesh, Y. Pei, X. Li, L. A. Curtiss and W. Huang, J. Am. Chem. Soc., 2017, **139**, 4762-4768.

7 P. Yang, X. Yuan, H. Hu, Y. Liu, H. Zheng, D. Yang, L. Chen, M. Cao, Y. Xu and Y. Min, Adv. Func. Mater., 2018, **28**, 1704774-1704782.

8 H. Huang, L. Ma, C. S. Tiwary, Q. Jiang, K. Yin, W. Zhou and P. M. Ajayan, Small, 2017, **13**. 1603013-1603021.

9 J. Zhang, X. Liu, A. Xing and J. Liu, ACS Appl. Mater. Interfaces, 2018, **1**, 2758-2768.

10 D. B. Gorle and M. A. Kulandainathan, J. Mater. Chem. A, 2017, **5**, 15273-15286.

11 L.G. Chen, X. Liang, X.T. Li, J.J. Pei, H. Lin, D.Z. Jia, W.X. Chen, D.S. Wang and Y.D. Li, Nano Energy, 2020, **73**, 104784-104791.

12 L. Huang, X. Zhang, Q. Wang, Y. Han, Y. Fang, S. Dong, J. Am. Chem. Soc., 2018, **140**, 1142-1147.

13 G.F. Hu, L. Shang, T. Sheng, Y.G. Chen and L.Y. Wang, Adv. Funct. Mater., 2020, **30**, 2002281-2002290.

14 Q. Wang, S. Chen, H. Lan, P. Li, X. Ping, S. Ibraheem, D. Long, Y. Duan and Z. Wei, J. Mater. Chem. A, 2019, **7**, 18143-18149.

15 D. V. Dao, T. D. Le, G. Adilbish, I.-H. Lee and Y.-T, Yu, J. Mater. Chem. A, 2019, **7**, 26996-

27006.

16 J. Liu, M. Jiao, B. Me, Y.X. Tong, Y.Q. Li, Mi.B. Ruan, P. Song, G.Q. Sun, L.H. Jiang, Y. Wang, Z. Jiang, L. Gu, Z. Zhou and W.L. X, Angew.Chem. Int.Ed., 2019, **58**,1163-1167.

17 S. Chen, Z. Niu, C. Xie, M. Gao, M. Lai, M. Li and P. Yang, ACS Nano, 2018, **12**, 8697-8705.

18 J. Liu, J. Bak, J. Roh, K.S. Lee, A. Cho, J. W. Han and E. Cho, ACS Catal., 2021, **11**, 466-475.

19 J. Liu, M.G. Jiao, L.L. Lu, H. M. Barkholtz, Y.Q. Li, Y. Wang and L.H. Jiang, Nat Commun., 2017, **8**, 15938-15948.

20 Y. Cai, P. Gao, F. Wang and H. Zhu, Electrochim. Acta, 2017, **245**, 924-933.

21 H. Wang, S. Yin, K. Eid, Y. Li, Y. Xu, X. Li, H. Xue and L. Wang, ACS Sustainable Chem. Eng. 2018, **6**, 11768-11774

22 X.j. Tang, D.h. Fang, L.j. Qu, D.Y. Xu, X.Q. Qin, B. Qin, W. Song, Z.G. Shao and B.L. Yi, Chinese J. Catal., 2019, **40**, 504-514.

23 X. X. Wang, S. Hwang, Y. T. Pan, K. Chen, Y. He, S. Karakalos, H. Zhang, J. S. Spendelow, D. Su and G. Wu, Nano Lett., 2018, **18**, 4163-4171.

24 Z.X. Liang, K. Nagamori, H. Igarashi, M. B. Vukmirovic, R. R. Adzic and K. Sasaki, ACS Catal., 2020, **10**, 4290-4298.

25 J.K. Zhao, H.Y. Su, H.L. Li, H.L. Wang, Z.P. Hu, J. Bao and J. Zeng, J. Am. Chem. Soc., 2021, **143**, 496-503.

26 Q. Wang, Q. Zhao, Y. Su, G. Zhang, G. Xu, Y. Li, B. Liu, D. Zheng and J. Zhang, J. Mater. Chem. A, 2016, **4**, 12296-12307.

27 T. Fu, J. Fang, C. Wang and J. Zhao, J. Mater. Chem. A, 2016, **4**, 8803-8811.

28 J.P. Perdew, K. Burke and M. Ernzerhof, Phys. Rev. Lett., 1996, **77**, 3865-3868.